Journal of Geophysical Research: Oceans

RESEARCH ARTICLE
10.1029/2018JC013855

Role of Baroclinic Processes on Flushing Characteristics in a Highly Stratified Estuarine System, Mobile Bay, Alabama

Jiabi Du[1,2], Kyeong Park[1], Jian Shen[2], Brian Dzwonkowski[3], Xin Yu[2], and Byung Il Yoon[4]

[1]Department of Marine Sciences, Texas A&M University, Galveston, TX, USA, [2]Virginia Institute of Marine Science, College of William and Mary, Gloucester Point, VA, USA, [3]Department of Marine Sciences, University of South Alabama, Dauphin Island, AL, USA, [4]Department of Ocean Sciences, College of Natural Science, Inha University, Incheon, South Korea

Key Points:
- Baroclinic processes, particularly the density-driven circulation, are important in the flushing of the stratified estuary
- Without the baroclinic processes, the flushing time can be overestimated by onefold under low to moderate river discharge conditions
- This is the first study to summarize the full three-dimensional general circulation in Mobile Bay, whose pattern is primarily regulated by river discharge and modulated by wind forcing

Correspondence to:
J. Du,
jdu@tamug.edu;
jiabi.du@gmail.com

Citation:
Du, J., Park, K., Shen, J., Dzwonkowski, B., Yu, X., & Yoon, B. I. (2018). Role of baroclinic processes on flushing characteristics in a highly stratified estuarine system, Mobile Bay, Alabama. *Journal of Geophysical Research: Oceans*, *123*, 4518–4537. https://doi.org/10.1029/2018JC013855

Received 30 JAN 2018
Accepted 29 MAY 2018
Accepted article online 8 JUN 2018
Published online 2 JUL 2018

Abstract Flushing of an estuary quantifies the overall water exchange between the estuary and coastal ocean and is crucially important for water quality as well as biological and geochemical processes within the system. Flushing times and freshwater age in Mobile Bay were numerically calculated under realistic and various controlled forcing conditions. Their responses to external forcing were explained by the three-dimensional characteristics of general circulation in the system. The flushing time ranges from 10 to 33 days under the 25th–75th percentile river discharges, nearly half of the previous estimates based on barotropic processes only, suggesting the important contribution of baroclinic processes. Their influence, quantified as the "new ocean influx," is on the same order of the river discharge under low to moderate river discharge conditions. The baroclinic influence increases and then decreases with increasing river discharge, aligning with the response of horizontal density gradient. By enhancing the net influx from the ocean mainly through density-driven circulation, baroclinic processes contribute to reduce flushing times. The three-dimensional circulation, which differs greatly between the wet and dry seasons, explains the temporal and spatial variations of the flushing characteristics. Wind forcing influences the three-dimensional circulation in the system with easterly and northerly winds tending to reduce the flushing time, while southerly and westerly winds the opposite.

1. Introduction

Flushing of an estuarine system indicates the renewal efficiency of a water body and quantifies its overall exchange with the coastal ocean. Flushing capacity in an estuary has long been of interest to oceanographers because it is crucially important for water quality, biological and ecosystem functions, sedimentation, pollutant dispersion, and geochemical processes (Alber & Sheldon, 1999; Choi & Lee, 2004; Du et al., 2018; Du & Shen, 2017; Lucas et al., 2009; Nixon et al., 1996). For instance, algal blooms depend on not only nutrient loads and external physical forcings such as temperature and solar radiation but also the flushing rate relative to the net growth rate (Garcon et al., 1986; Lehrter, 2008). Even in systems with no significant nutrient load, slow water exchange rates can result in coastal eutrophication and harmful algal blooms (Bricelj & Lonsdale, 1997; Lindahl et al., 1998; Nordberg et al., 2001; Rosenberg, 1990). Understanding the flushing, particularly how it responses to changes in external forcing and physical conditions, is essential for biological and ecosystem research as well as water quality management.

To quantify the flushing, several transport timescales have been used. Among them, flushing time, residence time, and water age are the three fundamental concepts (Alber & Sheldon, 1999; Bolin & Rodhe, 1973; Delhez et al., 2014; Monsen et al., 2002; Takeoka, 1984; Zimmerman, 1988). These timescales have been widely used in applications in a variety of estuaries (Abdelrhman, 2005; Du & Shen, 2015, 2016; Sheldon & Alber, 2006; Shen & Haas, 2004; Viero & Defina, 2016). Flushing time, the average time of materials to stay within a system before being flushed out, is a bulk or integrative parameter that describes the overall renewal capability of a waterbody and it establishes the time scale for physical transport of river-borne material, such as nutrients, organic matter, and suspended sediment (Dyer, 1973; Geyer et al., 2000; Officer, 1976; Oliveira & Baptista, 1997; Rayson et al., 2016). It can thus be compared against the time scales of relevant biogeochemical processes to determine whether transformations are occurring in estuaries (Alber & Sheldon, 1999).

There are commonly two classes of methods to estimate this timescale, one based on volume and flux and the other based on time series of tracer concentrations. The first class of approaches has been widely

employed because of its simplicity and has been modified over time to improve its typically coarse nature. The most basic form of the volume and flux approach assumes well-mixed and steady state conditions and represents the flushing time (τ_f) as

$$\tau_f = V/Q_t \tag{1}$$

where V is the total volume and Q_t is the total net flux (Alber & Sheldon, 1999; Asselin & Spaulding, 1993; Fischer et al., 1979). The formula is modified for estuarine application as the freshwater fraction method,

$$\tau_f = V_f/Q_f \tag{2}$$

where V_f is the freshwater volume based on observed data or simulated salinity field and Q_f is the freshwater input (Dyer, 1973; Huang, 2007). This method implicitly includes the coastal ocean input, but it may overestimate the flushing time if the freshwater input is very small. For low freshwater input systems, a tidal prism method may be more suitable. The tidal prism method is similarly based on volume-flux relationships and expresses the flushing time as

$$\tau_f = VT/[(1-\beta)P] \tag{3}$$

where P is the tidal prism, T is period of the tidal cycle, and β is the return ratio, which is the fraction of returning water during the flood tide to the total water flushed out during the previous ebb tide (Andutta et al., 2013; Dyer, 1973; Kuo et al., 2005; Sanford et al., 1992). The return ratio is the critical parameter in the tidal prism method and can be estimated based on the measurements of salinity at the estuary-ocean boundary during both ebb and flood tides (Fischer et al., 1979; Moore et al., 2006).

The other class of approach for determining flushing time is to use numerical models to simulate the time series of tracer mass and record the time when the mass decreases to a certain level (Ahmed et al., 2017; Hong & Shen, 2012). Models vary in sophistication from simple zero-dimensional (box) to elaborated three-dimensional ones (Abdelrhman, 2005; Hagy et al., 2000). When released within a domain of interest, the material concentration decreases with time, usually following an exponential function. Flushing time is commonly defined as the time necessary for a concentration to decrease to 1/e (~0.37) of its initial concentration (Deleersnijder et al., 2001; Dyer, 1973). Flushing time under this definition is therefore also known as the *e*-folding time. To calculate flushing time, both Lagrangian particle and Eulerian dye simulations have been applied in previous studies (e.g., Hong & Shen, 2012; Monsen et al., 2002). Using particle tracking, diffusion and turbulence's impacts need to be parameterized, which are usually addressed by adding a random walk property to the particles (Andutta et al., 2013; Webb & Marr, 2016). The Lagrangian method may overestimate flushing time by not accounting for diffusion, which is an important property for most soluble or even particulate materials (Burwell et al., 2000).

The flushing of a given system depends on the estuarine-shelf exchange (barotropic and baroclinic) and is a complicated function of geometry, bathymetry, wind, tide, and freshwater discharge (Choi & Lee, 2004; Kampf & Ellis, 2015; Kim & Park, 2012). Among them, freshwater discharge, tide, and wind are most important controls on system flushing, and their relative dominance can shift seasonally. For well-mixed estuaries, especially those with large tidal ranges and shallow bathymetry, tides are commonly the dominant factor through the tidal pumping mechanism (Chadwick & Largier, 1999; Fischer et al., 1979), while for partially mixed and stratified estuaries, moderate to large freshwater water discharge induces baroclinic processes that augment the flushing (Du & Shen, 2016). Baroclinic processes include persistent, seasonal, or periodic estuarine circulations in both along-estuary and cross-estuary directions, which have been proved to cause notable influence in water exchange (Du, 2017; MacCready & Geyer, 2010). These circulation patterns result in distinctively different material fates depending on the depth of particle releases, regardless of material settling properties. Additional forcing conditions and physical processes modulating the flushing include upwelling, wind-driven circulation, and wind-induced coastal Ekman transport, all of which can cause dramatic changes in water exchange over relatively short time periods (Feng & Li, 2010; Park, Valentine, et al., 2007). Estuarine circulation has long been recognized to modulate the estuarine water exchange with the coastal ocean (Fischer, 1972; Hansen & Rattray Jr., 1965; Knudsen, 1900; Takeoka, 1984; Warner et al., 2010). The influence of estuarine circulation on the exchange processes, however, is not easy to quantify. MacCready (2011) proposed the concept of "total exchange flow" (TEF) to describe the subtidal flux

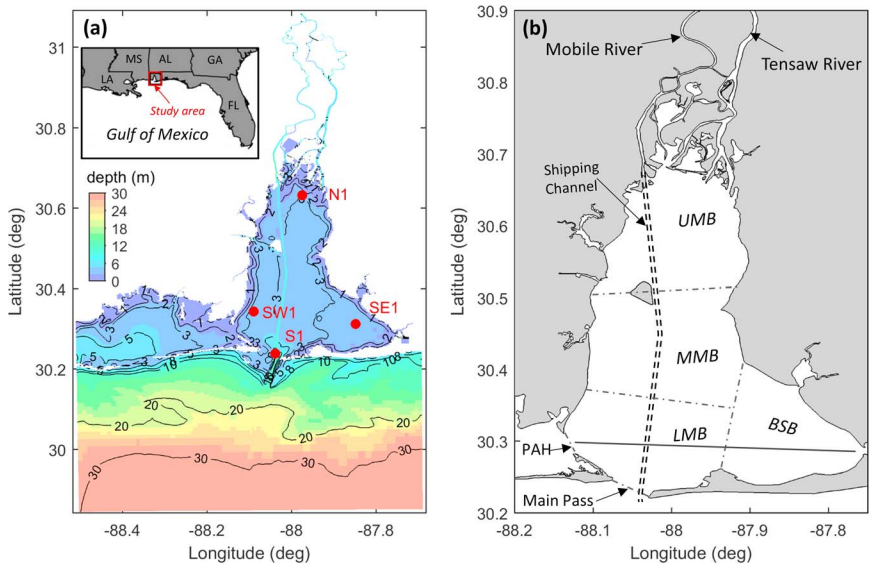

Figure 1. (a) Bathymetry of Mobile Bay and its adjacent coastal ocean and (b) a map of Mobile Bay. In (a), the color indicates the bathymetry and the red dots denote the four selected stations (N1, S1, SE1, and SW1) and the insert shows the location of Mobile Bay in the northern Gulf of Mexico. In (b), the dot-dashed lines separate the different regions of the Upper Mobile Bay (UMB), Middle Mobile Bay (MMB), Lower Mobile Bay (LMB), and Bon Secour Bay (BSB) and the solid line in the lower bay denotes a cross-channel section shown in Figure 14. The double dashed line in (b) indicates the ship channel.

integrated over a salinity range (i.e., in isohaline coordinate), which yields an exchange flow including both tidal and subtidal flux and satisfied the Knudsen relation (Knudsen, 1900). Chen et al. (2012) applied this concept and compared the isohaline exchange flow with the conventional Eulerian quantity, suggesting that the exchange flow in short estuaries could be more dependent on tidal volume flux instead of the baroclinic pressure gradient.

In this study, we choose Mobile Bay, a shallow and stratified estuary that receives large river discharge, to further explore the effects of baroclinic processes on flushing characteristics in estuarine systems. The hydrodynamics in Mobile Bay are known to vary with season because of large variations in river discharge and wind-induced vertical mixing (Dzwonkowski et al., 2011; Park, Kim, et al., 2007), allowing for a wide range of naturally occurring conditions to be tested. Because of the small tidal range, shallow system depth, and large river input, previous studies on the flushing of Mobile Bay have focused on the importance of river discharge, but neglected the potential influence of density-driven circulation (Schroeder et al., 1990; Webb & Marr, 2016). Our study, the first one in Mobile Bay focusing on the role of baroclinity on system flushing characteristics, demonstrates that this forcing component has profound impacts, especially during periods with high stratification. We used a well-calibrated three-dimensional hydrodynamic model to calculate the flushing time based on multiple dye release experiments under different discharge and wind conditions. The freshwater age was computed for a two-year period covering both low and high river discharge periods to examine the spatial and temporal variation of the flushing characteristics in this shallow, yet stratified estuarine system.

2. Materials and Methods

2.1. Study Area, Mobile Bay

Mobile Bay, located in the northern Gulf of Mexico, is a shallow and broad estuary (Figure 1). It has a mean depth of 3 m, with a deep (12–14 m) and narrow (120 m) ship channel extending from the mouth to the Port of Mobile (Dzwonkowski et al., 2011; Kim & Park, 2012). It has a volume of 3.2×10^9 m^3 and a surface area of 985 km^2 (Dinnel et al., 1990). While the bay itself is relatively large, approximately 50 km in length (north-south) and 14–34 km in width (east-west), its connections to the Gulf and Mississippi Sound are narrow and shallow. The water exchange with the northern Gulf is mainly through two outlets, Main Pass in the south and

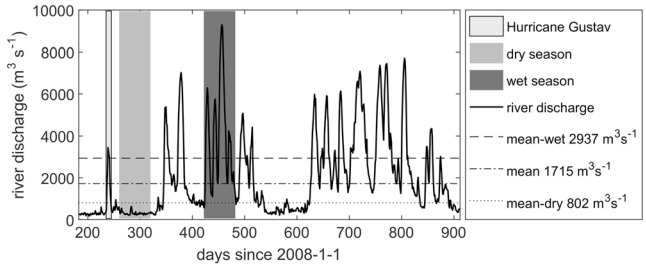

Figure 2. River discharge during the two-year base model simulation. The periods of interest are marked with filled rectangles, including the Hurricane Gustav and two selected 60-day periods representing the typical dry (days 260–320) and wet (days 422–482) seasons. The river discharge values of mean low (25th percentile), median, and mean high (75th percentile) conditions are indicated with horizontal lines.

Pass-aux-Herons (PAH) in the southwest, which on average account for 64% and 36% of the water exchange, respectively (Kim & Park, 2012).

Mobile Bay receives a mean river discharge of 1,677 m^3/s, the fourth largest discharge in the continental United States and the second largest in the Gulf of Mexico following the Mississippi River, from a drainage area of 115,000 km^2 covering Alabama, Mississippi, Georgia, and Tennessee (Dinnel et al., 1990). The bay receives 95% of its freshwater input from the Mobile River system, including Mobile and Tensaw Rivers (Kim & Park, 2012). It also receives 4.7 metric million tons of sediment (mostly silt and clay) per year (Mobile Bay National Estuary Program, 2002), of which 70% are deposited in the basin and the remaining 30% are exported to the shelf in the south and Mississippi Sound in the west (Byrnes et al., 2013; Cordi et al., 2003; Isphording et al., 1996). Over 42,000 tons of nitrogen enters the bay annually (Mobile Bay National Estuary Program, 2002).

Wind is an important forcing in shallow Mobile Bay and shows distinct seasonal variation. A southerly wind is dominant in spring and summer, and a stronger northerly wind is dominant in fall and winter (Noble et al., 1996). The tide is predominantly diurnal with a mean tidal range of 0.4 m and the tidal range varies from $<$0.1 m during equatorial tides to 0.8 m during tropic tides (Schroeder et al., 1990). The tidal prism for each diurnal cycle is estimated to be 4×10^8 m^3 based on our calculation of the flux across the two outlets, which is nearly the same as that determined by the product of mean tidal range and the basin area.

Despite the shallow bathymetry, strong vertical stratification has been persistently observed in Mobile Bay (Park, Kim, et al., 2007; Park et al., 2014; Schroeder et al., 1990). Vertical salinity differences as high as 19 psu over a vertical distance of 2.5 m have been observed in the northern portion of the bay (Park, Kim, et al., 2007). Strong vertical salinity gradients of 4–6 psu/m have also been observed in the southern portion of the bay (Ha & Park, 2012). Stratification levels change significantly between wet and dry seasons. During the extremely high-flow periods (e.g., river discharge $>$6,000 m^3/s), the entire bay is mainly freshwater dominated and vertically mixed with the exception of deep ship channel, which remains stratified (Schroeder et al., 1990). In contrast, the low- to moderate-flow periods typically have water column stratification very sensitive to the wind condition because of shallow bathymetry (Ryan et al., 1997; Schroeder et al., 1990). However, the horizontal salinity gradients likely induce a gravitational circulation and thus allow the water column to quickly restratify once wind is diminished (Park, Kim, et al., 2007; Schroeder et al., 1990). Highly stratified conditions are persistently observed during summer when the wind speed is commonly small, resulting in an isolated bottom water and regular episodes of multiday hypoxia (Park, Kim, et al., 2007; Turner et al., 1987). The variability in salinity (density) gradients that induce baroclinic processes in Mobile Bay makes it an ideal estuary for our study.

2.2. Numerical Model Simulations

We used a well-validated three-dimensional hydrodynamic model to study the flushing of Mobile Bay. The hydrodynamics model is based on the Three-dimensional Hydrodynamic-Eutrophication Model (HEM3D), also referred to as the Environmental Fluid Dynamics Code (EFDC; Hamrick, 1992). The model domain includes Mobile Bay, the Mobile River system, eastern Mississippi Sound, and the adjacent shelf (Figure 1a). The modeling domain is 80 km $\times$ 136 km in the east-west and north-south directions, respectively. The seaward open boundary is extended southward to about 45 km south of Dauphin Island, and the upriver boundary is at Mount Vernon (about 48 km to the north of the Mobile, AL). The grid system has 21,705 surface water cells and five vertical sigma layers, with the grid size varying from 58 to 2,000 m. The finest grid cells are small enough to resolve the narrow ship channel, represented by three continuous grid indices to ensure a more accurate simulation of mass transport along the channel (Kim & Park, 2012). The model application, being forced by realistic freshwater input, wind, and open boundary conditions for water level and salinity, gave a good reproduction of the observed water level, current velocity, and salinity for both tidal and subtidal components. Detailed information of the model configuration and its application and validation can be found in Kim and Park (2012) and Park et al. (2014). The numerical model run for two years from July 2008 to June 2010, which covered two wet and two dry seasons, served as the base for the estimation of the freshwater age (Figure 2). The model validation for salinity over the same two-year period was presented in Park

Table 1
Experimental Design and Flushing Time Under Each Forcing Condition

ID	Description	Forcing			Simulation period	Flushing time[a] (day)	
		Wind	Flow (m^3/s)	Open boundary water level			
Base	Realistic forcing	Real	Real	Real	2008.7 to 2010.6	NA	
F00	Zero flow	Random[b]	0	harmonic	300 days	269.0	
F05	5th percentile flow	Random	235	harmonic	100 days	44.7	
F10	10th percentile flow	Random	280	harmonic	100 days	41.3	
F20	20th percentile flow	Random	375	harmonic	100 days	35.5	
F25	25th percentile flow	Random	426	harmonic	100 days	32.9	(36.1, 29.6)
F30	30th percentile flow	Random	489	harmonic	100 days	30.0	
F40	40th percentile flow	Random	658	harmonic	100 days	25.1	
F50	50th percentile flow	Random	906	harmonic	100 days	19.7	(22.2, 17.5)
F60	60th percentile flow	Random	1,268	harmonic	100 days	15.9	
F70	70th percentile flow	Random	1,808	harmonic	100 days	12.0	
F75	75th percentile flow	Random	2,199	harmonic	100 days	10.2	(12.0, 8.7)
F80	80th percentile flow	Random	2,694	harmonic	100 days	8.8	
F90	90th percentile flow	Random	4,361	harmonic	100 days	5.9	
F95	95th percentile flow	Random	5,850	harmonic	100 days	4.8	
Fm	Mean flow	Random	1,677	harmonic	100 days	12.6	(14.6, 10.8)
F8 k	8,000 flow	Random	8,000	harmonic	100 days	5.1	
F10 k	10,000 flow	Random	10000	harmonic	100 days	4.2	
W1	Easterly wind	5 m/s E	1,677	harmonic	15 days	10.3	(11.2, 9.5)
W2	Westerly wind	5 m/s W	1,677	harmonic	15 days	13.2	(14.2, 12.3)
W3	Southerly wind	5 m/s S	1,677	harmonic	15 days	14.3	(14.4, 14.2)
W4	Northerly wind	5 m/s N	1,677	harmonic	15 days	10.9	(12.5, 9.1)

[a]Flushing time with dye released throughout the water column (in bottom and surface layers). [b]Random wind has a constant speed of 5 m/s and a random direction varying from 0 to 360°, with the direction changing every 3 hr.

et al. (2014). We selected two 60-day periods representing the typical dry (days 260–320) and wet (days 422–482) seasons for our analysis.

2.3. Flushing Time Calculation and Experimental Setup

To calculate flushing time, Eulerian dye simulations were conducted using the hydrodynamic model under controlled conditions of river discharge and wind (Table 1). Dye is released as a passive tracer, whose transport equation is the same as for salt-balance equation involving advective transport, turbulent diffusive transport, and source-sink terms except that it will not influence the density field,

$$\frac{\partial C}{\partial t} + \nabla\left(\vec{u}C\right) = \frac{\partial}{\partial z}\left(\kappa\frac{\partial C}{\partial z}\right) + F_h \tag{4}$$

where C is tracer concentration, $\vec{u}$ is velocity field, κ is vertical eddy diffusivity, and F_h is horizontal diffusion and mass sources/sinks. Radiation boundary was applied for the dye mass computation.

For all simulations, dye was released over the entire water column for the main bay (UMB + MMB + LMB + BSB in Figure 1). Additional runs with dye released in bottom layers (lower 40% of the depth) and surface layers (upper 40% of the depth) were conducted for mean low flow (25th percentile, 426 m^3/s), median flow (906 m^3/s), mean flow (1,677 m^3/s), mean high flow (75th percentile, 2,199 m^3/s), and different wind conditions (W1 to W4 in Table 1). The low (25th percentile) and high (75th percentile) flows were considered to represent the mean dry and wet seasons, respectively, based on the statistical analysis of 42-year (1976–2017) historical data at U.S. Geological Survey (USGS) gauge stations (USGS 02428400 and USGS 02469761). For idealized simulations with different river discharges, we applied a wind with the speed of 5 m/s (close to long-term mean) with the wind direction changing randomly every 3 hr. In each idealized case, dye was released after 60 days of model run to ensure a stable density field.

Idealized runs for different wind forcing condition were conducted to examine the impact of wind on flushing. Four wind conditions with a constant speed of 5 m/s blowing from east, west, south, and north for a

period of 15 days were tested under mean river discharge condition. Dye was released one day after the wind forcing was applied. Most of the wind energy falls between 2 and 12 days in Mobile Bay (Noble et al., 1996). Short-term wind forcing duration does not fully reach the flushing criteria (i.e., the *e*-folding value), and we thus chose a wind duration that is slightly longer than typical conditions in the system but should robustly resolve the flushing time scales. It is important to note that wind forcing with a shorter period can also influence the water exchange through wind-induced flushing, with its influence affected by estuarine geometry and bathymetry (Geyer, 1997).

2.4. Water Mass Budget

Water mass inside a semienclosed estuarine system is renewed by not only the freshwater discharge from the ambient watersheds but also the coastal ocean water input. Depending on the tidal and wind forcing and the density field, the influence of the coastal ocean varies. Using the flushing time (τ_f), the contributions from freshwater discharge (Q_f) and coastal ocean water (Q_o) were isolated through a simple mass balance equation (Guo & Lordi, 2000; MacCready, 2011),

$$Q_t = \frac{V}{\tau_f} \tag{5}$$

$$Q_o = Q_t - Q_f \tag{6}$$

where Q_t is total net outflow and Q_o is the tidally averaged net influx of new water from the coastal ocean, hereinafter referred to as "new ocean influx." The term "new" water indicates the water that is new to the system, excluding the returning portion of the water flushed out during the previous ebb tide. From a mass balance perspective, the volume of new water during one tidal cycle can also be regarded as "escaping volume" (Ketchum, 1951). A portion of the water flushed out during the previous tidal cycle could reenter the system, which is regarded as "old" water.

The Q_o results from the combination of pure tidal exchange and baroclinic-induced flow, quantifying the overall contribution from coastal ocean on the flushing of an estuarine system (Lemagie & Lerczak, 2015; Takeoka, 1984). However, it is challenging to directly calculate Q_o as the return ratio varies temporally and among different systems. Note that Q_o is different from the residual bottom landward flux of the gravitational circulation. However, we show in this study that they are positively related.

2.5. Water Age Calculation

In addition to flushing time, which gives a bulk metric representative of the overall flushing of the system, freshwater age was also computed to examine the spatial and temporal variations of the flushing inside the bay. Age of a water parcel at a given location is defined as the time elapsed since the parcel enters the defined water body through one of the defined boundaries (Deleersnijder et al., 2001; Takeoka, 1984; Zimmerman, 1976). Water age was calculated using the method in Delhez et al. (1999), which has been widely employed for many estuaries (Du et al., 2017; Karna & Baptista, 2016; Shen & Wang, 2007; Zhang et al., 2010). The freshwater age is computed based on two variables, the tracer concentration C and age concentration α. Assuming that there is only one tracer released to the system without internal sources and sinks, the transport equation for computing the tracer and the age concentration can be written as (Deleersnijder et al., 2001; Delhez et al., 1999)

$$\frac{\partial C(t,\vec{x})}{\partial t} + \nabla\left[\vec{u}C(t,\vec{x}) - K\nabla C(t,\vec{x})\right] = 0 \tag{7}$$

$$\frac{\partial \alpha(t,\vec{x})}{\partial t} + \nabla\left[\vec{u}\alpha(t,\vec{x}) - K\nabla C(t,\vec{x})\right] = C(t,\vec{x}) \tag{8}$$

where $\nabla = \vec{i}\frac{\partial}{\partial x} + \vec{j}\frac{\partial}{\partial y} + \vec{k}\frac{\partial}{\partial z}$ and K is the diffusivity tensor that takes into account of the turbulent motions. The tracer concentration C is calculated in the same way as general passive tracers are calculated, while the age concentration α increases by $C{\cdot}\Delta t$ at every time step. The mean age can then be calculated as follows,

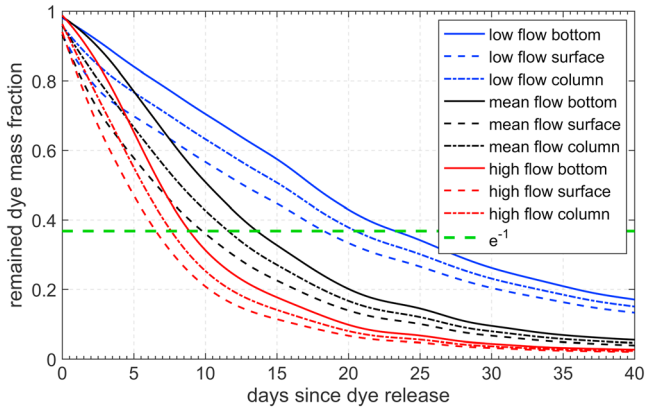

Figure 3. The subtidal time series of the simulated dye mass fraction inside Mobile Bay for different river flow conditions (low, median, and high flows) and different release depths (surface layers, bottom layers, and entire water column).

$$\tau_a\left(t, \overrightarrow{x}\right) = \frac{\alpha\left(t, \overrightarrow{x}\right)}{C\left(t, \overrightarrow{x}\right)} \quad (9)$$

Age calculation module (equations (7)–(9)) implemented in the EFDC model has been successfully applied for many coastal systems (e.g., Hong & Shen, 2012; Shen & Haas, 2004).

3. Results

3.1. Flushing Time

The estimated water column flushing (*e*-folding) times are 32.9, 19.7, 12.6, and 10.2 days for mean low (426 m^3/s), median (906 m^3/s), mean (1,677 m^3/s), and mean high (2,199 m^3/s) river flows, respectively (Table 1 and Figure 3). Depending on the release type (over the entire water column, in the upper 40% of the depth, or in the lower 40% of the depth), the flushing times of surface and bottom waters differ by 3.3–6.5 days, which is equivalent to about 20–32% of the flushing times for entire water column release. For a given river discharge, flushing times are highest when released in bottom layers and lowest when released in surface layers. The differences can be attributed to strong stratification and gravitational circulation. A portion of the bottom water mass can be transported into the upper estuary due to gravitational circulation and thus may have a longer retention time.

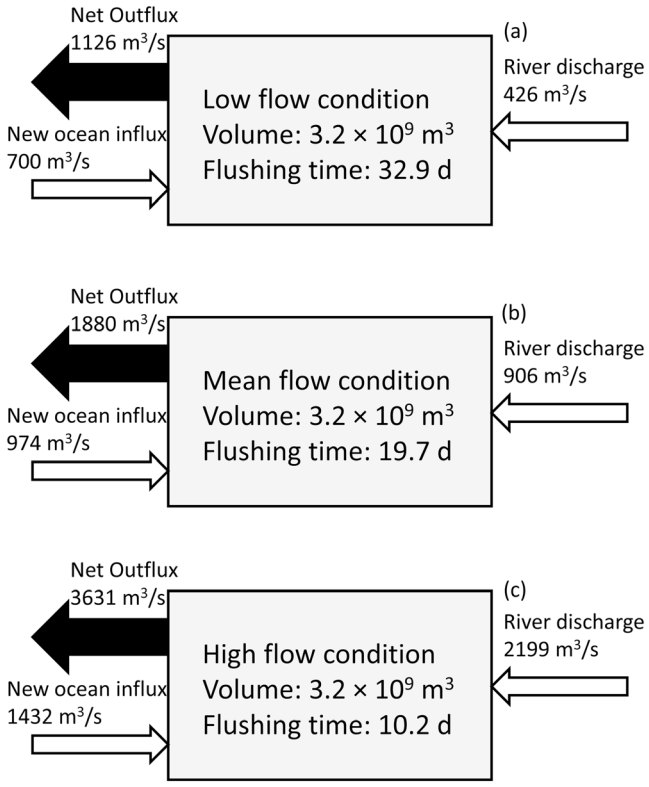

Figure 4. Water mass budget for low (25th percentile), median, and high (75th percentile) river flow conditions based on the flushing time calculation. The net outflux is the bay water volume divided by the flushing time, and the difference between net outflux and river discharge is the "new ocean influx."

Under the wind forcing from different directions and constant mean river flow, the water column flushing times vary from 10.3 to 14.3 days (Table 1). Northerly and easterly winds tend to reduce the flushing time by pushing the water toward south and west, increasing the outflow through the Main Pass and PAH, respectively. Interestingly, even though Main Pass serves as the main outlet of the bay (Kim & Park, 2012), it is the easterly, instead of the northerly, wind that is more effective in reducing the flushing time. The southerly and westerly winds tend to enlarge the flushing time, with the southerly wind resulting in the longest flushing time. The vertical difference of flushing time is smallest under southerly wind condition (0.2 day), and largest under northerly wind condition (3.4 days), indicating an enhanced vertical mixing by the southerly (up-estuary) wind and a strengthened stratification under northerly (down-estuary) wind condition, consistent with the study of wind's impact on estuarine circulation (Chen & Sanford, 2009).

3.2. Water Mass Flux Based on Flushing Time

With the calculated flushing times, the coastal ocean's contribution to the flushing of the bay can be estimated based on the water budget model as the first-order approximation (equations (5) and (6)). The fluxes of new ocean water (Q_o) are 700, 974, and 1,432 m^3/s for low-, median-, and high-flow conditions, respectively, demonstrating that the coastal ocean's contribution to the flushing of the system is on the same order of river discharge (Figure 4). The coastal ocean's input increases with river discharge, but its relative contribution, that is, Q_o relative to Q_f, decreases with increasing river discharge. Examination of the full spectrum of river discharge (0–10,000 m^3/s) shows Q_o increases and then decreases with increasing river flow (see section 4.1).

Having the volume of new water during each diurnal cycle ($V_{new} = Q_oT$), we can estimate the return ratio

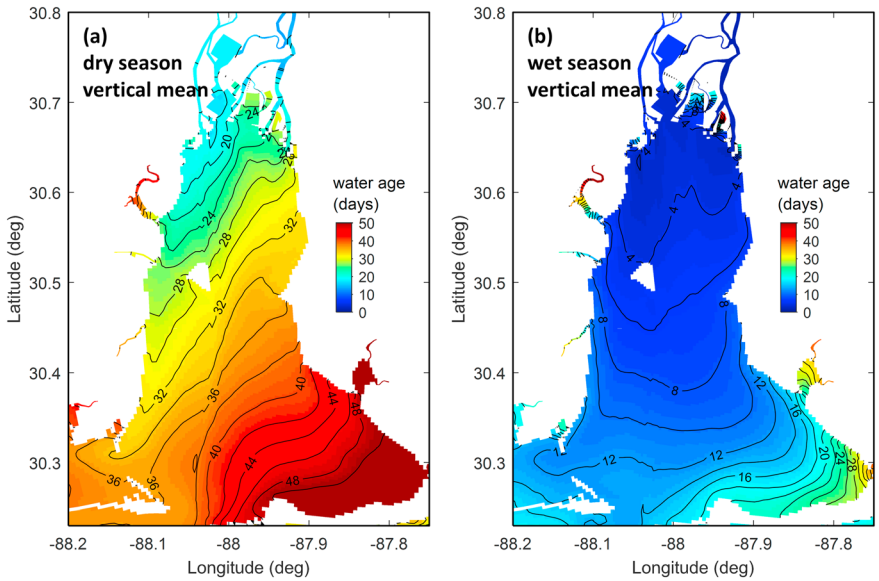

Figure 5. Vertical mean freshwater age inside Mobile Bay for (a) dry and (b) wet seasons: see Figure 2 for the two selected 60-day periods for the dry and wet seasons.

$$\beta = 1 - \frac{V_{\text{new}}}{P} \tag{10}$$

The mean tidal prism over one diurnal cycle was estimated to be about 4×10^8 m^3 per diurnal cycle, given the mean tidal range of 0.4 m and an area of 985 km^2. The estimated tidal prisms are close to the computation from the model calculated flux through the two outlets, Main Pass and PAH. The similar values in the tidal prism between the two methods are due to the relatively short estuary length (50 km) relative to the diurnal tidal wavelength (473 km with a mean depth of 3 m). The new ocean water influx that ranges from 700 m^3/s under low-flow condition to 1,432 m^3/s under high-flow condition (Figure 4) gives a return ratio ranging from 70% to 85%, with a larger return ratio under lower flow condition.

3.3. Spatial Variation of the Freshwater Age

Unsurprisingly, there is a significant seasonal difference in freshwater age (Figure 5). The vertical mean freshwater ages averaged over the main bay were 34 and 9 days for the selected dry and wet seasons, respectively (see Figure 2 for the two selected 60-day periods). The larger freshwater age within the bay during the dry season was mainly attributable to two processes. One was the longer transport time from the headwater to the upper bay, 18 days compared to 3 days during the wet season (Figure 5). The other was the longer transport time within the bay during the dry season. Materials released from the upper bay took 20 and 10 days to reach the bay mouth for dry and wet seasons, respectively, based on the differences in water age between the mouth and the upper bay (Figure 5).

The spatial pattern of the freshwater age is quite interesting (Figure 5). Freshwater age was highly asymmetric across the bay during the dry season, with a smaller freshwater age along the western bay compared to the eastern bay. During the wet season, on the other hand, there was a much weaker east-west asymmetry in the freshwater age, with the freshwater age slightly larger along both shores and smaller in the middle, which may relate to the influence of lateral baroclinic motion (Smith, 1977). This indicates that freshwater moved faster along the western side of the bay during the dry season, while freshwater moved faster in the middle and slower on either side during the wet season. For both wet and dry seasons, the freshwater age was largest in the southeastern part of the bay. In the most southeastern portion of Bon Secour Bay, freshwater age could reach 54 days during the dry season and 30 days during the wet season. Water age gradient was highest in this region during wet season, suggesting a rather slow exchange of water in Bon Secour Bay.

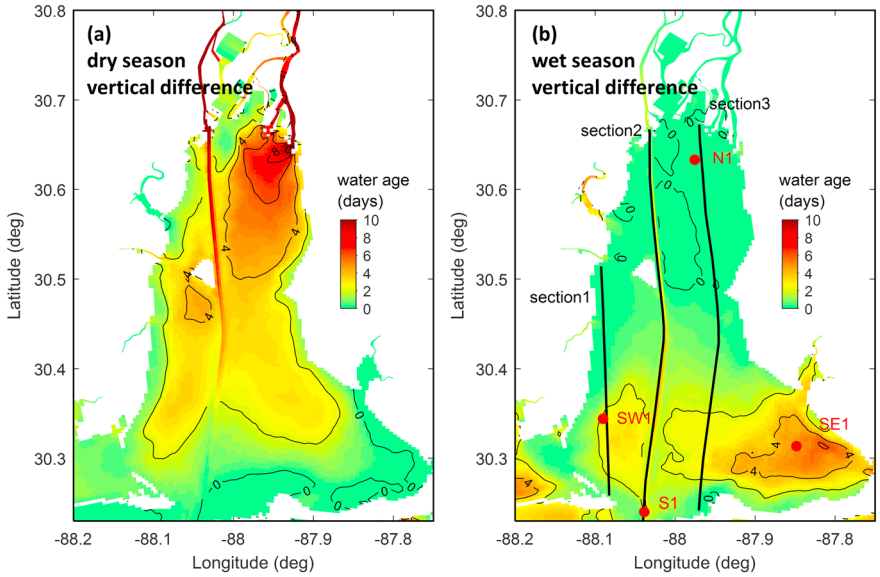

Figure 6. The vertical (bottom-surface) difference of the freshwater age for (a) dry and (b) wet seasons. In (b), the solid lines denote the three along-bay sections shown in Figure 7 and the red dots denote the four selected stations (N1, S1, SE1, and SW1).

The vertical difference (bottom-surface) of the water age varied in accordance with the seasonally varying strength of stratification. Interestingly, the largest vertical difference occurred in distinctively different regions during different seasons, that is, the northeast and the southeast region of the bay during the dry and wet seasons, respectively (Figure 6). The vertical difference is evident in the vertical profiles of the water age along the three along-bay sections (Figure 7). Except for the deep ship channel, the upper and middle bays were well-mixed during the wet season, resulting in little vertical difference in the freshwater age. During the dry season, however, the vertical shear extended into the upper bay. In the deep ship channel, the vertical shear always existed regardless of the flow condition, aligning with the persistently strong salt intrusion and density stratification in the ship channel. The vertical profiles of the freshwater age are similar to those of salinity, but the vertical shear of freshwater age is usually smaller than that of salinity, particularly along the deep ship channel (Figure 7).

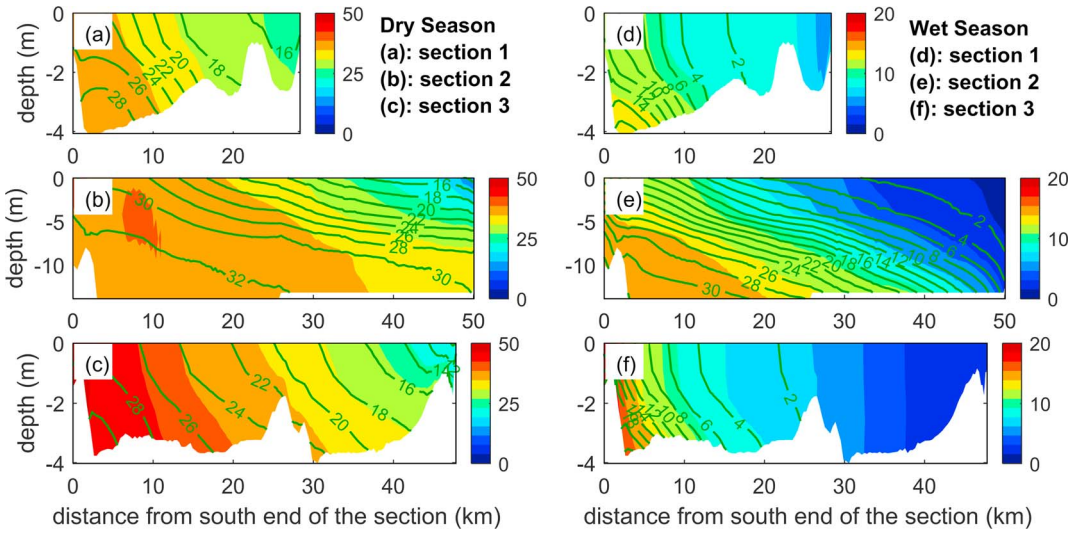

Figure 7. Vertical profiles of the freshwater age (filled color) and salinity (green contour lines) during (left panels) dry and (right panels) wet seasons for the three along-bay sections: see Figure 6 for the section locations. Note that section 2 is along the ship channel.

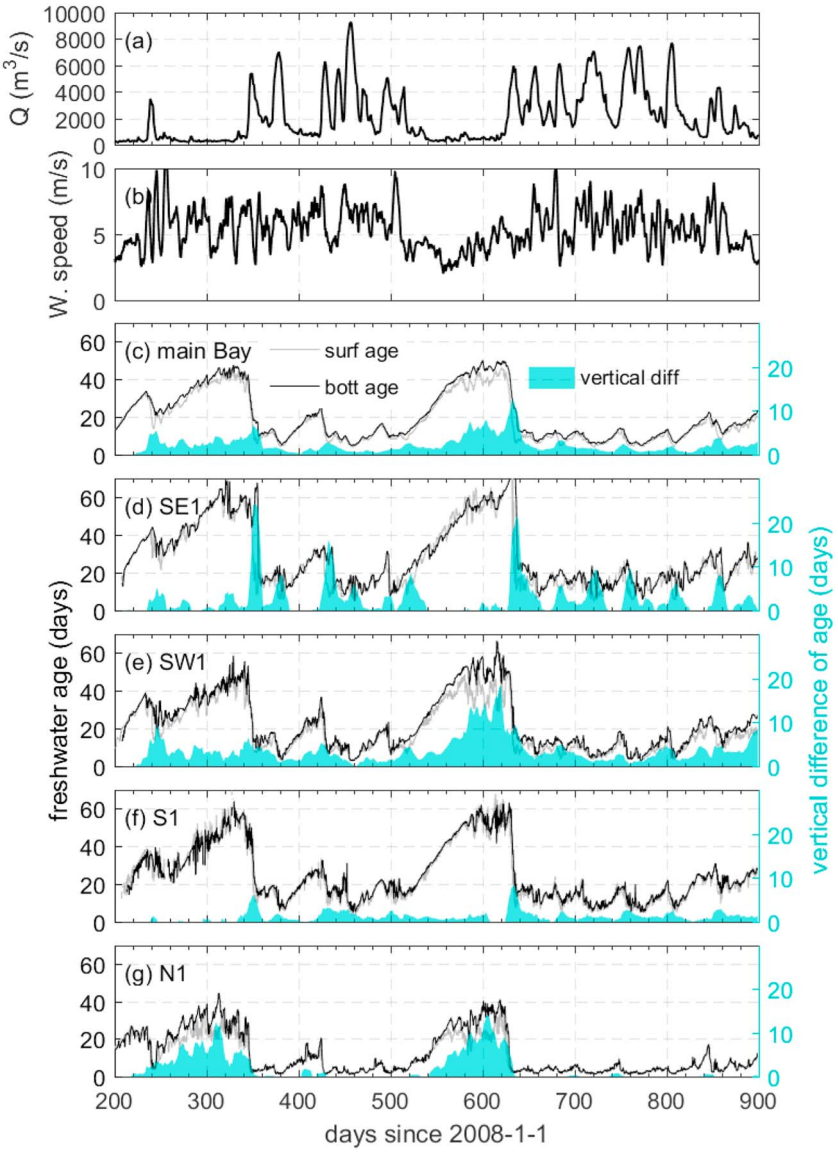

Figure 8. Temporal variation of (a) river discharge, (b) wind speed, and (c) freshwater age averaged over the main bay and at (d–g) the selected four stations shown in Figure 1a for surface water (grey line), bottom water (black line), and the vertical (bottom-surface) difference (cyan area).

3.4. Temporal Variation of the Freshwater Age

The freshwater age shows high temporal variability over the two-year simulation period, mainly in response to the varying freshwater discharge (Figure 8). The mean freshwater age averaged vertically and over the main bay ranged from 5 days in the wet season to 50 days in the dry season (Figure 8c). The mean freshwater age increased gradually until to a certain value during the dry season; it decreased quickly during the transition from the dry to wet season, and it remained low during the wet season. Occasionally, a pulse of freshwater discharge during the dry season (typically summer and fall) due to storm events caused a quick decrease in water age, for example, Hurricane Gustav on days 245–255. Similarly, with a relatively small river discharge lasting for tens of days during the wet season, the water age increased gradually, as seen around day 400.

The vertical difference of freshwater age also varied with wind speed (Figure 8). Over the two-year run, a larger vertical difference occurred during the dry seasons and a maximum vertical difference occurred

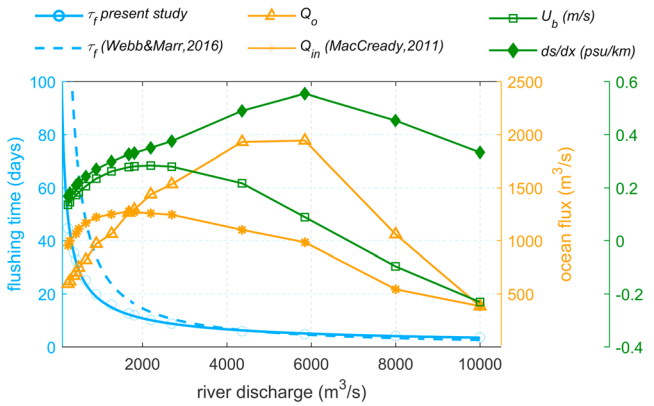

Figure 9. Flushing time (τ_f), new ocean water influx (Q_o), total exchange flow (Q_{in}) using the isohaline method in MacCready (2011), residual bottom velocity averaged along the ship channel (U_b: positive northward), and horizontal salinity gradient (d*s*/d*x*) along the ship channel as a function of freshwater discharge. Markers denote the model results from the numerical experiments, and the blue solid line represents the best exponential fit, while the blue dashed line represents the flushing time estimation based on a vertically integrated numerical model (Eq. 3 in Webb & Marr, 2016).

during the second dry season on days 525–625, which was evident in the main bay and station SW1 and N1. The vertical difference in the main bay exceeded 10 days during the second dry season, larger than that during the first dry season, which could be attributed to the weaker wind in the second dry season (Figure 8b). At station SE1 (Bon Secour Bay), the vertical difference was generally small but had multiple peaks with values exceeding 20 days (Figure 8d). The vertical difference persisted at station SW1, with values larger than 20 days in the second dry season (Figure 8e). Interestingly, the vertical difference of water age was very small at station S1 (Figure 8f), which might be related to the strong vertical mixing induced by the relatively strong tidal current near the narrow outlet, that is, Main Pass. Different from other stations, N1 showed virtually no vertical difference during the wet season but relatively large vertical difference during the dry season (Figure 8g). Located at the northernmost section of the bay, the entire water column of N1 was dominated by freshwater during wet seasons, resulting in negligible vertical difference in water age. During dry seasons, a well-established estuarine circulation moved water with larger age from the lower bay to the north, which combined with stratification resulted in a large vertical difference in water age at station N1.

4. Discussion

4.1. Processes Contributing to System Flushing

For a semienclosed estuarine system, water exchange is mainly composed of three components, river discharge, tidal exchange, and baroclinic flow induced by the density gradient. Their relative importance varies greatly among different systems, depending on the tidal range, magnitude of freshwater input, and the estuarine geometry and bathymetry. Wind forcing typically modulates the primary exchange mechanisms; however, in some systems, it can be a dominant factor (Feng & Li, 2010; Geyer, 1997; Kang et al., 2017). System flushing for an estuary is derived from both river and ocean inputs. Even within the same system, the main forcing can shift from a tidal dominance near the mouth to river flow dominance near the head of an estuary. For a well-mixed estuary with limited river discharge, the water exchange or flushing is dominated by tidal pumping and the system is primarily flushed by oceanic waters (Kampf & Ellis, 2015), while for a partially mixed estuary, estuarine circulation can play a more important role (Chen et al., 2012; Du & Shen, 2016; MacCready, 2011). While baroclinic forcing is known to be an important circulation feature (Li et al., 1998; Valle-Levinson, 1995), quantification of its relative role on flushing, particularly in shallow but stratified estuarine systems, has not been extensively studied. Our results show that the baroclinic processes in this highly stratified system are critically important in Mobile Bay. However, the relative dominance of these processes changes with time, depending on the variations in tidal range and river discharge as well as the wind forcing. These forcing interactions have a wide range of timescales from days to seasons.

River discharge is clearly very important in controlling flushing in Mobile Bay, and its influence can vary dramatically over time, consistent with previous work (e.g., Stumpf et al., 1993; Webb & Marr, 2016). The relative importance of river discharge, tide, wind, and baroclinic flow exhibits strong seasonal signals in Mobile Bay. We conducted multiple sensitivity runs to cover the full spectrum of river discharge (Table 1) and derived an empirical relationship for the flushing time over the entire main bay as a power function of river discharge,

$$\tau_f = 2320.2 \times Q_f^{-0.707} \tag{11}$$

where flushing time (τ_f) is in day and freshwater discharge (Q_f) is in m^3/s (Figure 9). The power relationship is mainly attributed to the nonlinear response of new ocean influx to river discharge. This relationship is different from the numerical model results based on a barotropic two-dimensional model by Webb and Marr (2016). The flushing calculated in the present study is about half of the value calculated by Webb and Marr (2016) under low to median river discharge condition, suggesting a strong influence of baroclinic

processes on the flushing. Both studies show high consistency when the flow is high (e.g., >4,000 m^3/s), due to the fresh status of the bay and strong vertical mixing.

While there is a clear link between river discharge and flushing time, the relative contribution of oceanic flushing plays an important role in this system. Using the water mass budget (equations (5) and (6)), we calculated the total outflux Q_t, and new ocean water influx Q_o. Under zero flow condition (not realistic) where the flushing is only controlled by tide, the flushing time is 269 days and the Q_o is only 137 m^3/s, suggesting an extremely low water exchange between the estuary and the ocean solely induced by tide. This results from the combination of limited tidal range (~0.4 m), narrow outlets, and large return ratios (97% from equation (10) for Q_o = 137 m^3/s). The Q_o increases with river flow in other simulations with different river discharges, which can be attributed to the baroclinic processes.

The relationships among river flow, baroclinic processes, and flushing times are further highlighted in Figure 9. Under low to moderate river flow condition (≤906 m^3/s), oceanic exchange (i.e., Q_o) is mainly derived from the baroclinic processes, which contributes nearly as much as freshwater discharge to the overall total outflux. The contribution from baroclinic processes subsequently decreases with increasing river discharge. Among the different river flow sensitivity runs, Q_o is maximum in the Case F95 (i.e., 5,850 m^3/s). Under extremely high flow condition (e.g., 10,000 m^3/s), the flushing is mainly regulated by river discharge and the oceanic exchange is highly limited.

The pattern of Q_o changing with river discharge coincides with the response of horizontal salinity gradient (ds/dx) along the ship channel (Figure 9). The horizontal salinity gradient drives gravitational circulation, and its value determines the strength of baroclinic current. Both Q_o and ds/dx are maximum in Case F95, showing consistent response to changing river discharge. The baroclinic current driving the landward bottom transport is the major component contributing to the new ocean influx. Note that change of Q_o is not consistent with the change in bottom residual velocity (U_b) averaged over the ship channel, which peaks around 2,000 m^3/s. Bottom residual velocity is the combination of the barotropic flow due to river discharge-induced surface slope and the baroclinic flow. Over extremely high river discharge (e.g., >8,000 m^3/s), the bottom baroclinic flow is overwhelmed by the barotropic flow, resulting in a seaward bottom residual velocity (Figure 9).

In comparison, we calculated the TEF over two sections across the two outlets using the isohaline framework method proposed by MacCready (2011), which was first applied in the Columbia River Estuary and found to be a precise way to calculate the landward transport (Chen et al., 2012). In this method, tidally averaged volume flux of water with salinity greater than s is defined as

$$Q(s) = \left\langle \int_{A_s} u dA \right\rangle \tag{11}$$

where A_s is the tidally varying portion of the cross section with salinity larger than s. In practice, we calculate $Q(s)$ for limited salinity bins from 0 to 35 with an interval of 1. Volume flux in a specific salinity class is defined as

$$-\frac{\partial Q}{\partial s} = -\lim_{\delta s \to 0} \frac{Q(s+\delta s/2) - Q(s-\delta s/2)}{\delta s} \tag{12}$$

where the minus sign indicates that a positive value of $-\partial Q/\partial s$ corresponds to inflow for a given salinity class.

$$Q_{in} \equiv \int \frac{-\partial Q}{\partial s}\Big|_{in} ds \tag{13}$$

Q_{in} is referred to as TEF, indicating the flux of water into the estuary due to all tidal and subtidal processes. Comparison between Q_{in} and Q_o estimated from flushing time shows that they are not consistent (Figure 9). Q_{in} follows the shape of bottom residual currents' (U_b's) response to river discharge, and its peak occurs around the mean river discharge (1,677 m^3/s). The fluxes of new ocean water (Q_o) are the first-order approximation of the fluxing, which appears that it does not exactly equal to the TEF. This discrepancy can be expected. Q_o is used as a proxy for the exchange rate, but it has the limitation to use it to estimate the exchange flow. It suggests that not all new water transported into estuary is by exchange flow. Water

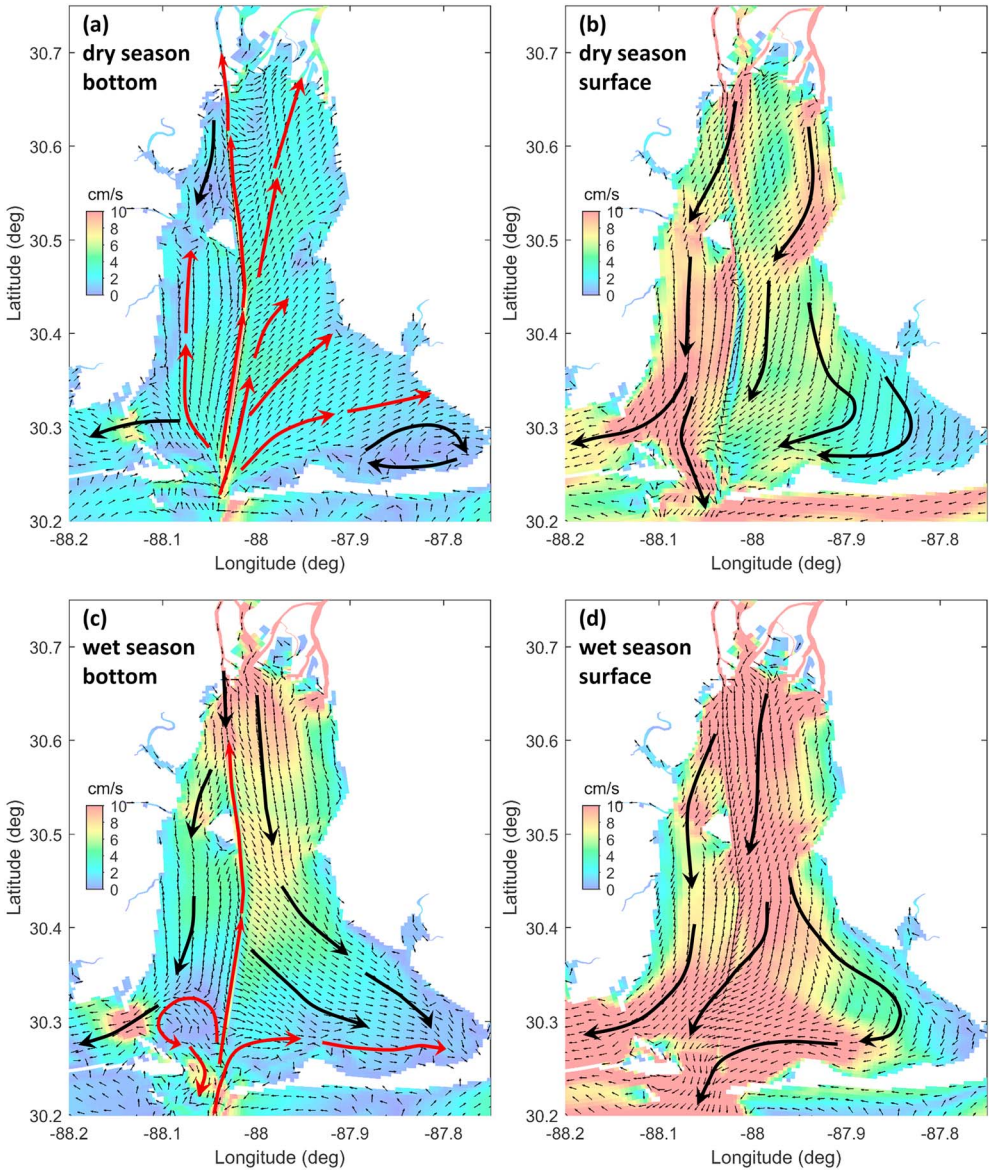

Figure 10. Bottom and surface residual current during the (a and b) dry and (c and d) wet seasons (see Figure 2 for the two selected 60-day periods), with the filled color denoting the current speed and the arrows denoting schematically the movement of high saline coastal ocean water (red) and fresher estuarine water (black).

exchange between the deep channel and the shallow areas is relatively slow and may not be reflected on the salt flux over the narrow mouth.

4.2. Residual Circulation and Its Role on System Flushing

The circulation pattern in Mobile Bay varied seasonally with freshwater discharge (Figure 10). During the dry season, bottom inflow could reach as far as the northern end of the bay and was slightly stronger on the eastern side of the bay. Meanwhile, the surface residual flow was stronger on the western side of the bay. The pattern was distinctively different for the wet season, during which the bottom residual flow was mostly in the downstream direction, with the exception of the narrow and deep ship channel and the lower bay. Contrary to the dry season, the downstream surface outflow was stronger on the eastern side of the bay during the wet season. In addition, an interesting lateral circulation was evident in the lower bay during both the wet and dry seasons, with a bottom flow toward the east and surface flow toward the west.

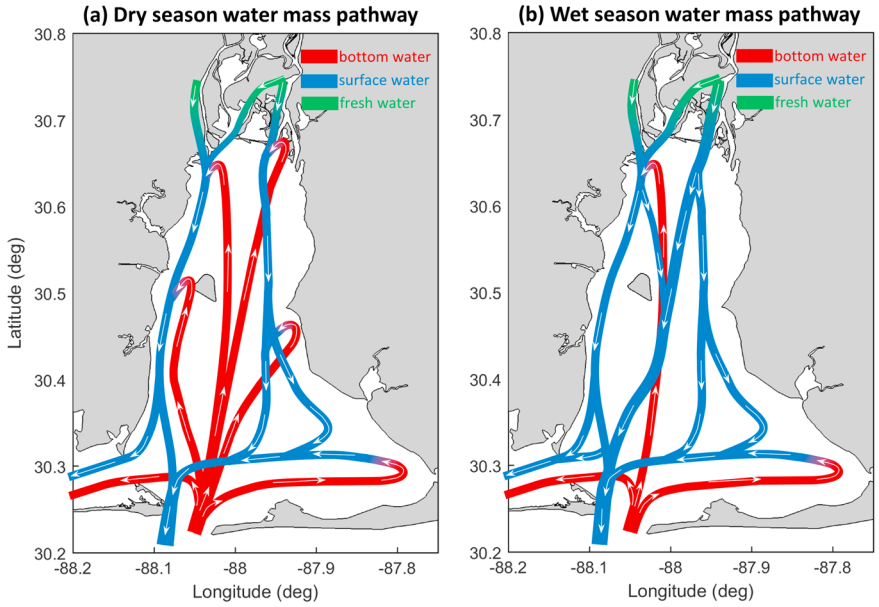

Figure 11. Sketch diagrams showing the pathway of bottom and surface water mass for typical (a) dry and (b) wet seasons. Note that the northward bottom residual current exists along the ship channel in both dry and wet seasons.

Sketch diagrams summarizing the major pathways of bottom and surface water are presented in Figure 11. Coastal ocean bottom water comes into the bay through Main Pass and spreads in three general directions: to the upper bay, to the east into Bon Secour Bay, and to the west into Mississippi Sound. Bottom water is mixed up to the surface during the transport and is exported out of the bay along with the freshwater that tends to be constrained in the surface layer. On average, the bay gains salt through Main Pass and loses about the same amount through PAH (Kim & Park, 2012). Depending on the freshwater discharge, the salt intrusion length differs, with a longer salt intrusion length during the dry season and much shorter intrusion during the wet season. During the dry season, bottom water can reach as far as the northern end of the bay not only in the deep ship channel but also in the shallow regions, whereas the bottom inflow exists only in the deep ship channel during the wet season. Even though the asymmetry of tidal straining may contribute to subtidal circulation, it is very unlikely to be important in this system given the small tidal range. The two-layer circulation is believed to be mainly driven by the density gradient. Density-driven current is most evident in the ship channel due to its deep depth, as the baroclinic pressure gradient at the bottom is directly determined by the horizontal density gradient and the total depth. During the wet season, in the shallow regions, the baroclinic pressure gradient is weak because of the shallow depth and is overwhelmed by the barotropic pressure gradient, resulting in a southward current over the entire water column in the shallow regions (Figure 11b).

The circulation patterns explain the spatial structure of the flushing characteristics in Mobile Bay. The flushing within a given region is determined by the net residual influx or outflux through all the boundaries. The largest values and horizontal gradients of freshwater age in Bon Secour Bay (Figure 5) indicate a slow flushing and can be attributed to the slowest residual current (Figure 10). The large vertical difference of age at station SE1 is believed to be caused by the persistent lateral circulation in this region. The residual current is much smaller during the dry season, compared to the wet season, explaining the very large freshwater age in Bon Secour Bay during the dry season ($>$50 days in Figure 5). The lateral circulation, which moves the water from the lower bay to Bon Secour Bay through the bottom layer, results in a larger water age in the bottom layer. The asymmetry in the water age between the wet and dry seasons in different regions, especially in the western and eastern parts of Mobile Bay, can also be attributed to the dramatic change in the residual current patterns between different seasons. Although the residual current in both the eastern and western parts are enhanced with increasing freshwater discharge, the residual current in the east is enhanced by a much greater magnitude, which causes the water age in the east to decrease quickly to almost the same value as in the west, resulting in a symmetric pattern of the water age during the wet season (Figure 5b).

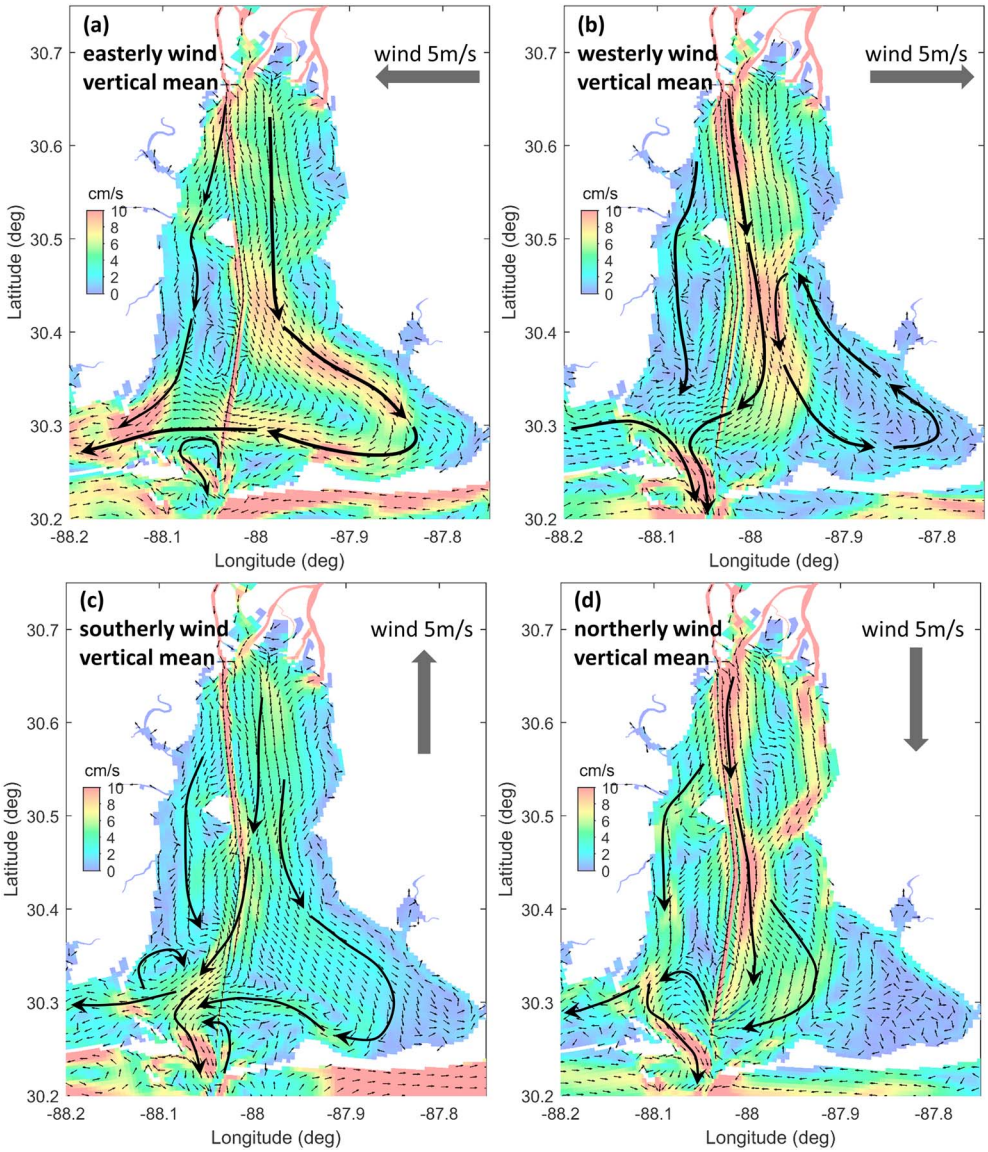

Figure 12. Vertical mean residual current for (a) easterly, (b) westerly, (c) southerly, and (d) northerly wind conditions, with filled color denoting the current speed. In all of the four experiments, a constant mean freshwater discharge of 1,677 m^3/s was applied and the wind blowing from one direction at a constant speed of 5 m/s for 15 days (see Table 1). The black arrows denote schematically the major characteristics of the circulation patterns.

Previous work in partially mixed estuarine systems have identified the importance of freshwater input and the resulting horizontal density gradient on generating density-driven circulation (e.g., MacCready, 2004; Pritchard, 1952; Valle-Levinson, 2008). The magnitude of circulation is linearly related with the salinity gradient and usually increases with freshwater discharge as found in Chesapeake Bay, a typical partially mixed estuary (Du & Shen, 2016). However, it is not the case in Mobile Bay. With a large freshwater discharge (e.g., $>$5,000 m^3/s), the entire bay is mainly dominated by freshwater. Even the salinity gradient in the ship channel appears to decrease under very high river flow conditions. As a result, the subtidal landward bottom flow in the upper bay during the dry season shifts southward in the wet season, consistent with the finding of Noble et al. (1996). This leads to vertically homogeneous freshwater age in the upper bay during the wet season. That is, the seasonal variability in the density-driven circulation has a large impact on the seasonal changes in the flushing characteristics in Mobile Bay.

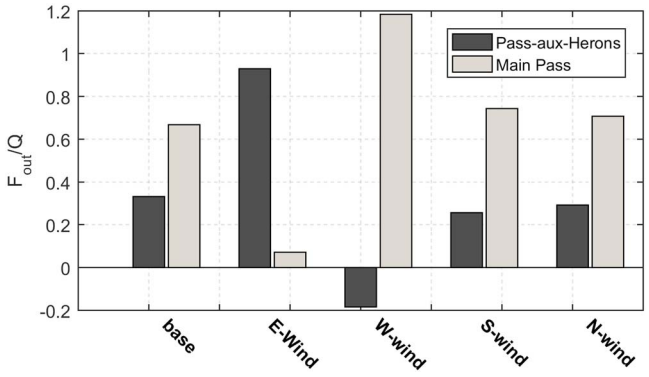

Figure 13. Net flux through the two main outlets of Mobile Bay, Main Pass and Pass-aux-Herons, under different wind forcing conditions. The net flux is normalized by the freshwater discharge, with positive (negative) value denoting a net outflux from (influx into) the bay.

4.3. Impact of Wind on the Circulation and Flushing

The impact of wind on estuarine circulation is well studied, and its effect on system flushing capacity depends on the forcing itself (i.e., wind speed and direction) as well as the characteristics of the system (e.g., morphology and stratification; Chen & Sanford, 2009; Geyer, 1997; Goodrich, 1988). The idealized model runs using different wind directions demonstrate the importance of this forcing on the residual circulation in the bay. In addition to a barotropic response, the three-dimensional representation of the bay allows the baroclinic response to be analyzed.

Winds forcing from different directions change the barotropic circulation (i.e., vertical mean residual circulation) greatly in Mobile Bay (Figure 12). Existence of two outlets, Main Pass and PAH, cause a unique response in the barotropic circulation to wind forcing, particularly the westerly and easterly wind. The estuarine water is typically exported through both Main Pass and PAH, which on average account for 64% and 36% of the outflow, respectively (Kim & Park, 2012). However, under some wind conditions, the relative importance of two outlets can change and the flux direction can even been reversed. For instance, with an easterly wind, a larger portion of estuarine water is exported through the PAH (~90%), leaving only a small percentage of estuarine water exported through the Main Pass (~10%; Figures 12a and 13). Conversely, with a westerly wind, water moves eastward through the PAH into the bay (opposite to normal conditions), strengthening the outflow through the Main Pass to about 120%, relative to the river discharge (Figures 12b and 13). While southerly and northerly winds, the dominant winds in Mobile Bay, have little impact on the export of the estuarine water (Figure 13), they influence the local circulation patterns and the residual current field. Northerly wind tends to increase the residual flow near the ship channel, while southerly wind tends to weaken the lateral variations (Figures 12c and 12d). The change in barotropic circulation, however, does not change the total net outflow and therefore has limited impact on the overall flushing

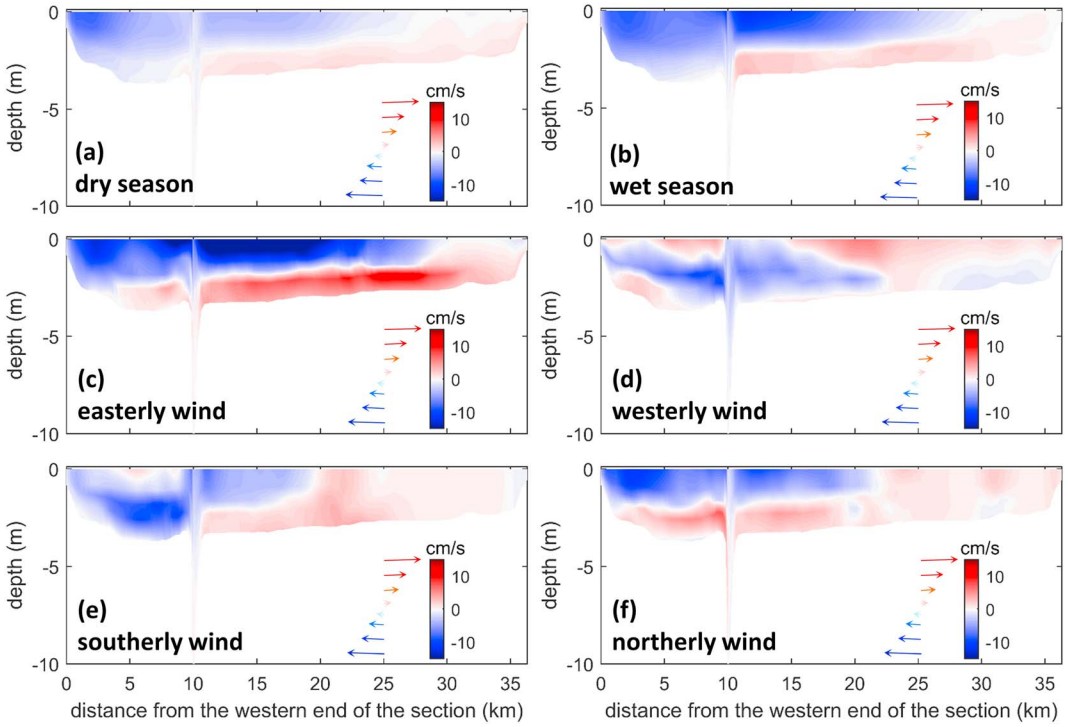

Figure 14. The vertical profiles of cross-bay residual current along the lower bay section (location shown in Figure 1b) for different forcing conditions. The filled color denotes the magnitude of the cross-bay current speed, with the red color indicating eastward current and the blue color indicating westward current.

capacity of the estuary, despite the fact that the localized change of barotropic circulation has high potential to alter the flushing in local areas.

The influence of wind on flushing is more associated with the two layer estuarine circulation in both longitudinal and lateral directions. A downstream wind enhances the surface outflow, which is compensated by an increased bottom inflow, resulting in a faster flushing. For example, in Chesapeake Bay, downstream wind could reduce the mean residence time by more than 10% (Du & Shen, 2016). For Mobile Bay, the downstream (northerly) wind reduces the flushing time by 13% compared to the mean flow condition (Table 1). Interestingly, the easterly wind is most effective in reducing the flushing time (by about 18%). This could be attributed to the strengthened lateral circulation in the lower bay (Figure 14c). With easterly wind, surface westward and bottom eastward residual currents are larger than 15 cm/s, much larger than those under other wind forcing conditions. The enhanced circulation across the lower bay could efficiently enhance the overall flushing of the bay, as Bon Secour Bay is an extremely low flushing area with very small vertical mean residual current and water age accumulating much faster in it than in other areas.

Both the barotropic and baroclinic response to wind forcing in Mobile Bay had significant impacts on system exchange and flushing. While the change in barotropic circulation alters water mass pathways and local flushing, the change in baroclinic circulation is the major mechanism through which the overall flushing of an estuary responses.

5. Conclusions

The flushing characteristics and associated residual circulation were investigated in Mobile Bay, a shallow but stratified estuary, using a three-dimensional hydrodynamic model. Comparison between the wet and dry seasons as well as idealized cases demonstrates the important contribution of baroclinic processes on the flushing capacity despite the shallow depth of the system (mean depth of 3 m). Vertical differences in the flushing time as well as the spatial variation of freshwater water age are influenced by the system density field and the resulting residual circulation. While the flushing time is found to be exponentially correlated with river flow, with the flushing time deceasing with increasing discharge, the relative importance of the baroclinic forcing is more complex. Using the new ocean influx as a proxy for the baroclinic contribution, it is shown that under low to moderate river flow conditions, the inflow from the oceanic boundary is as important to system flushing as river flow. Overall, the impact of baroclinic processes leads to about 50% reduction in flushing time compared to the estimates based on a depth-integrated two-dimensional model.

In examining the temporal and spatial patterns in the flushing characteristics, the seasonal variations in the general circulation of Mobile Bay are identified. Surprisingly, to our knowledge, this is the first study to describe the full three-dimensional general circulation in Mobile Bay. The seasonal changes in flushing characteristics are directly related to the changes in the general circulation patterns with the landward bottom flow being severely restricted in its extent during the wet season. In addition, two distinct flow patterns contribute to the estuary-ocean water exchange (i.e., along and across system circulation cells). These circulations are regulated by river discharge and modulated by the wind field. Northerly and easterly winds tend to enhance the estuarine-ocean exchange by strengthening the density-driven circulation, while westerly and southerly winds tend to weaken the system flushing. Overall, this study highlights the important control of baroclinic processes on the system flushing and suggests that using river flow or tidal prism to estimate flushing time may have some limits, especially in stratified coastal systems. We demonstrate that using a three-dimensional numerical model with the baroclinic processes is best suited for examining the flushing characteristics in shallow stratified systems.

Acknowledgments
This publication was supported by the U.S. Department of Commerce's National Oceanic and Atmospheric Administration under NOAA Award NA14OAR4170098 and the Mississippi-Alabama Sea Grant Consortium. The first author is supported by the institutional fellowship at Texas A&M University at Galveston. We thank two reviewers for their constructive comments. The data sets used in this study have been made available at http://doi.org/10.5281/zenodo.1221412.

References

Abdelrhman, M. A. (2005). Simplified modeling of flushing and residence times in 42 embayments in New England, USA, with special attention to Greenwich Bay, Rhode Island. *Estuarine, Coastal and Shelf Science*, *62*(1-2), 339–351. https://doi.org/10.1016/j.ecss.2004.09.021

Ahmed, A., Pelletier, G., & Roberts, M. (2017). South Puget Sound flushing times and residual flows. *Estuarine, Coastal and Shelf Science*, *187*, 9–21. https://doi.org/10.1016/j.ecss.2016.12.027

Alber, M., & Sheldon, J. E. (1999). Use of a date-specific method to examine variability in the flushing times of Georgia estuaries. *Estuarine, Coastal and Shelf Science*, *49*(4), 469–482. https://doi.org/10.1006/ecss.1999.0515

Andutta, F. P., Ridd, P. V., & Wolanski, E. (2013). The age and the flushing time of the Great Barrier Reef waters. *Continental Shelf Research*, *53*, 11–19. https://doi.org/10.1016/j.csr.2012.11.016

Asselin, S., & Spaulding, M. (1993). Flushing times for the Providence River based on tracer experiments. *Estuaries*, *16*(4), 830–839. https://doi.org/10.2307/1352442

Bolin, B., & Rodhe, H. (1973). A note on the concepts of age distribution and transit time in natural reservoirs. *Tellus*, *25*(1), 58–62.

Bricelj, V. M., & Lonsdale, D. J. (1997). Aureococcus anophagefferens: Causes and ecological consequences of brown tides in U.S. mid-Atlantic coastal waters. *Limnology and Oceanography*, *42*(5part2), 1023–1038. https://doi.org/10.4319/lo.1997.42.5_part_2.1023

Burwell, D., Vincent, M., Luther, M., & Galperin, B. (2000). Modeling residence times: Eulerian vs Lagrangian. In M. L. Spaulding, & H. L. Butler (Eds.), *Estuarine and Coastal Modeling* (pp. 995–1009). Reston, VA: ASCE.

Byrnes, M. R., Berlinghoff, J. L., & Griffee, S. F. (2013). *Sediment dynamics in Mobile Bay, Alabama: Development of an operational sediment budget*. Mashpee, MS: Applied Coastal Research and Engineering, Inc.

Chadwick, D. B., & Largier, J. L. (1999). Tidal exchange at the bay-ocean boundary. *Journal of Geophysical Research*, *104*(C12), 29,901–29,924. https://doi.org/10.1029/1999JC900165

Chen, S.-N., Geyer, W. R., Ralston, D. K., & Lerczak, J. A. (2012). Estuarine exchange flow quantified with isohaline coordinates: Contrasting long and short estuaries. *Journal of Physical Oceanography*, *42*(5), 748–763. https://doi.org/10.1175/JPO-D-11-086.1

Chen, S.-N., & Sanford, L. P. (2009). Axial wind effects on stratification and longitudinal salt transport in an idealized, partially mixed estuary. *Journal of Physical Oceanography*, *39*(8), 1905–1920. https://doi.org/10.1175/2009JPO4016.1

Choi, K. W., & Lee, J. H. W. (2004). Numerical determination of flushing time for stratified water bodies. *Journal of Marine Systems*, *50*(3-4), 263–281. https://doi.org/10.1016/j.jmarsys.2004.04.005

Cordi, J. A., Meylan, M. A., & Isphording, W. C. (2003). Metal distribution and metal site partitioning, Mobile Bay surface sediments. *Transactions of the Gulf Coast Association of Geological Societies*, *53*, 145–159.

Deleersnijder, E., Campin, J.-M., & Delhez, E. J. M. (2001). The concept of age in marine modelling I. Theory and preliminary model results. *Journal of Marine Systems*, *28*, 229–267.

Delhez, E. J. M., Campin, J.-M., Hirst, A. C., & Deleersnijder, E. (1999). Toward a general theory of the age in ocean modelling. *Ocean Modelling*, *1*(1), 17–27. https://doi.org/10.1016/S1463-5003(99)00003-7

Delhez, É. J. M., de Brye, B., de Brauwere, A., & Deleersnijder, É. (2014). Residence time vs influence time. *Journal of Marine Systems*, *132*, 185–195. https://doi.org/10.1016/j.jmarsys.2013.12.005

Dinnel, S. P., Schroeder, W. W., & Wiseman, W. J. Jr. (1990). Estuarine-shelf exchange using Landsat images of discharge plumes. *Journal of Coastal Research*, *6*(4), 789–799.

Du, J. (2017). *Impact of climate variation and human adaptation on the physical transport processes and water exchange in Chesapeake Bay* (pp. 87–89). Gloucester Point, VA: College of William and Mary.

Du, J., & Shen, J. (2015). Decoupling the influence of biological and physical processes on the dissoved oxygen in the Chesapeake Bay. *Journal of Geophysical Research: Oceans*, *120*, 78–93. https://doi.org/10.1002/2014JC010422

Du, J., & Shen, J. (2016). Water residence time in Chesapeake Bay for 1980–2012. *Journal of Marine Systems*, *164*, 101–111. https://doi.org/10.1016/j.jmarsys.2016.08.011

Du, J., & Shen, J. (2017). Transport of riverine material from multiple rivers in the Chesapeake Bay: Important control of estuarine circulation on the material distribution. *Journal of Geophysical Research: Biogeosciences*, *122*, 2998–3013. https://doi.org/10.1002/2016JG003707

Du, J., Shen, J., Bilkovic, D. M., Hershner, C. H., & Sisson, M. (2017). A numerical modeling approach to predict the effect of a storm surge barrier on hydrodynamics and long-term transport processes in a partially mixed estuary. *Estuaries and Coasts*, *40*(2), 387–403. https://doi.org/10.1007/s12237-016-0175-0

Du, J., Shen, J., Park, K., Wang, Y. P., & Yu, X. (2018). Worsened physical condition due to climate change contributes to the increasing hypoxia in Chesapeake Bay. *Science of the Total Environment*, *630*, 707–717. https://doi.org/10.1016/j.scitotenv.2018.02.265

Dyer, K. R. (1973). *Estuaries: A physical introduction*. London, UK: Wiley.

Dzwonkowski, B., Park, K., Ha, H. K., Graham, W. M., Hernandez, F. J., & Powers, S. P. (2011). Hydrographic variability on a coastal shelf directly impacted by estuarine discharge. *Continental Shelf Research*, *31*(9), 939–950. https://doi.org/10.1016/j.csr.2011.03.001

Feng, Z., & Li, C. (2010). Cold-front-induced flushing of the Louisiana Bays. *Journal of Marine Systems*, *82*(4), 252–264. https://doi.org/10.1016/j.jmarsys.2010.05.015

Fischer, H. B. (1972). Mass transport mechanisms in partially stratified estuaries. *Journal of Fluid Mechanics*, *53*(4), 671–687. https://doi.org/10.1017/S0022112072000412

Fischer, H. B., List, E. J., Koh, R. C. Y., Imberger, J., & Brooks, N. H. (1979). *Mixing in inland and coastal waters*. San Diego, CA: Academic Press.

Garcon, V. C., Stolzenbach, K. D., & Anderson, D. M. (1986). Tidal flushing of an estuarine embayment subject to recurrent dinoflagellate blooms. *Estuaries*, *9*(3), 179–187. https://doi.org/10.2307/1352129

Geyer, W. R. (1997). Influence of wind on dynamics and flushing of shallow estuaries. *Estuarine, Coastal and Shelf Science*, *44*(6), 713–722. https://doi.org/10.1006/ecss.1996.0140

Geyer, W. R., Morrs, J. T., Pahl, F. G., & Jay, D. A. (2000). Interaction between physical processes and ecosystem structure: A comparative approach. In J. E. Hobbie (Ed.), *Estuarine science: A synthetic approach to research and practice* (pp. 177–206). Washington, DC: Island Press.

Goodrich, D. M. (1988). On meteorologically induced flushing in three U.S. East Coast estuaries. *Estuarine*, *26*, 111–121.

Guo, Q., & Lordi, G. P. (2000). Method for quantifying freshwater input and flushing time in estuaries. *Journal of Environmental Engineering*, *126*(7), 675–683. https://doi.org/10.1061/(ASCE)0733-9372(2000)126:7(675)

Ha, H. K., & Park, K. (2012). High-resolution comparison of sediment dynamics under different forcing conditions in the bottom boundary layer of a shallow, micro-tidal estuary. *Journal of Geophysical Research*, *117*, C06020. https://doi.org/10.1029/2012JC007878

Hagy, J. D., Boynton, W. R., & Sanford, L. P. (2000). Estimation of net physical transport and hydraulic residence times for a coastal plain estuary using box models. *Estuaries*, *23*(3), 328–340. https://doi.org/10.2307/1353325

Hamrick, J. M. (1992). *A three-dimensional environmental fluid dynamics computer code. Theoretical and computational aspects*. Gloucester Point, VA: Virginia Institute of Marine Science.

Hansen, D. V., & Rattray, M. Jr. (1965). Gravitational circulation in straits and estuaries. *Journal of Marine Research*, *23*, 104–122.

Hong, B., & Shen, J. (2012). Responses of estuarine salinity and transport processes to potential future sea-level in the Chesapeake Bay. *Estuarine, Coastal and Shelf Science*, *104-105*, 33–45. https://doi.org/10.1016/j.ecss.2012.03.014

Huang, W. (2007). Hydrodynamic modeling of flushing time in a small estuary of North Bay, Florida, USA. *Estuarine, Coastal and Shelf Science*, *74*(4), 722–731. https://doi.org/10.1016/j.ecss.2007.05.016

Isphording, W. C., Imsand, F. D., & Jackson, R. B. (1996). Fluvial sediment characteristics of the Mobile River Delta. *Transactions of the Gulf Coast Association of Geological Societies*, *46*, 185–191.

Kampf, J., & Ellis, H. (2015). Hydrodynamics and flushing of Coffin Bay, South Australia: A small tidal inverse estuary of interconnected bays. *Journal of Coastal Research*, *31*(2), 447–457.

Kang, X., Xia, M., Pitula, J. S., & Chigbu, P. (2017). Dynamics of water and salt exchange at Maryland Coastal Bays. *Estuarine, Coastal and Shelf Science*, *189*, 1–16. https://doi.org/10.1016/j.ecss.2017.03.002

Karna, T., & Baptista, A. M. (2016). Water age in the Columbia River estuary. *Estuarine, Coastal and Shelf Science*, *183*, 249–259. https://doi.org/10.1016/j.ecss.2016.09.001

Ketchum, B. H. (1951). The flushing of tidal estuaries. *Sewage and Industrial Wastes*, *23*(2), 198–209.

Kim, C.-K., & Park, K. (2012). A modeling study of water and salt exchange for a micro-tidal, stratified northern Gulf of Mexico estuary. *Journal of Marine Systems*, *96–97*, 103–115.

Knudsen, M. (1900). Ein hydrographischer Lehrsatz. *Annalen der Hydrographie und Maritimen Meteorologie*, *28*, 316–320.

Kuo, A. Y., Park, K., Kim, S.-C., & Lin, J. (2005). A tidal prism water quality model for small coastal basins. *Coastal Management*, *33*(1), 101–117. https://doi.org/10.1080/08920750590883015

Lehrter, J. C. (2008). Regulation of eutrophication susceptibility in oligohaline regions of a northern Gulf of Mexico estuary, Mobile Bay, Alabama. *Marine Pollution Bulletin*, *56*(8), 1446–1460. https://doi.org/10.1016/j.marpolbul.2008.04.047

Lemagie, E. P., & Lerczak, J. A. (2015). A comparison of bulk estuarine turnover timescales to particle tracking timescales using a model of the Yaquina Bay estuary. *Estuaries and Coasts*, *38*(5), 1797–1814. https://doi.org/10.1007/s12237-014-9915-1

Li, C., Valle-Levinson, A., & Wong, K. C. (1998). Separating baroclinic flow from tidally induced flow in estuaries. *Journal of Geophysical Research*, *103*(C5), 10,405–10,417. https://doi.org/10.1029/98JC00582

Lindahl, O., Belgrano, A., Davidsson, L., & Hernroth, B. (1998). Primary production, climatic oscillations, and physico-chemical processes: The Gullmar Fjord time-series data set (1985–1996). *ICES Journal of Marince Science*, *55*(4), 723–729. https://doi.org/10.1006/jmsc.1998.0379

Lucas, L. V., Thompson, J. K., Brown, L. R., Dallas, K., Foster, S., Monsen, N., & Schraga, T. (2009). Why are diverse relationships observed between phytoplankton biomass and transport time? *Limnology and Oceanography*, *54*(1), 381–390. https://doi.org/10.4319/lo.2009.54.1.0381

MacCready, P. (2004). Toward a unified theory of tidally-averaged estuarine salinity structure. *Estuaries*, *27*(4), 561–570. https://doi.org/10.1007/BF02907644

MacCready, P. (2011). Calculating estuarine exchange flow using isohaline coordinates. *Journal of Physical Oceanography*, *41*(6), 1116–1124. https://doi.org/10.1175/2011JPO4517.1

MacCready, P., & Geyer, W. R. (2010). Advances in estuarine physics. *Annual Review of Marine Science*, *2*(1), 35–58. https://doi.org/10.1146/annurev-marine-120308-081015

Mobile Bay National Estuary Program (2002). *Comprehensive conservation and management plan: A Call to Action* (Vol. 1). Mobile, AL: Mobile Bay National Estuary Program.

Monsen, N. E., Cloern, J. E., Lucas, L. V., & Monismith, S. G. (2002). The use of flushing time, residence time, and age as transport time scales. *Limnology and Oceanography*, *47*(5), 1545–1553. https://doi.org/10.4319/lo.2002.47.5.1545

Moore, W. S., Blanton, J. O., & Joye, S. B. (2006). Estimates of flushing times, submarine groundwater discharge, and nutrient fluxes to Okatee Estuary, South Carolina. *Journal of Geophysical Research*, *111*, C09006. https://doi.org/10.1029/2005JC003041

Nixon, S. W., Ammerman, J. W., Atkinson, L. P., Pilson, M. E. Q., & Seitzinger, S. P. (1996). The fate of nitrogen and phosphorus at the land-sea margin of the North Atlantic Ocean. *Biogeochemistry*, *35*(1), 141–180. https://doi.org/10.1007/BF02179826

Noble, M. A., Schroeder, W. W., Wiseman, W. J. Jr., Ryan, H. F., & Gelfenbaum, G. (1996). Subtidal circulation patterns in a shallow, highly stratified estuary: Mobile Bay, Alabama. *Journal of Geophysical Research*, *101*(C11), 25,689–25,703. https://doi.org/10.1029/96JC02506

Nordberg, K., Filipsson, H. L., Gustafsson, M., Harland, R., & Roos, P. (2001). Climate, hydrographic variations and marine benthic hypoxia in Koljö Fjord, Sweden. *Journal of Sea Research*, *46*(3-4), 187–200. https://doi.org/10.1016/S1385-1101(01)00084-3

Officer, C. B. (1976). *Physical oceanography of estuaries (and associated coastal waters)*. New York: Wiley.

Oliveira, A., & Baptista, A. M. (1997). Diagnostic modeling of residence time in estuaries. *Water Resources Research*, *33*(8), 1935–1946. https://doi.org/10.1029/97WR00653

Park, K., Kim, C.-K., & Schroeder, W. W. (2007). Temporal variability in summertime bottom hypoxia in shallow areas of Mobile Bay, Alabama. *Estuaries and Coasts*, *30*(1), 54–65. https://doi.org/10.1007/BF02782967

Park, K., Powers, S. P., Bosarge, G. S., & Jung, H. (2014). Plugging the leak: Barrier island restoration following Hurricane Katrina enhances larval retention and improves salinity regime for oysters in Mobile Bay, Alabama. *Marine Environmental Research*, *94*, 48–55. https://doi.org/10.1016/j.marenvres.2013.12.003

Park, K., Valentine, J. F., Sklenar, S., Weis, K. R., & Dardeau, M. R. (2007). The effects of Hurricane Ivan in the inner part of Mobile Bay, Alabama. *Journal of Coastal Research*, *23*, 1332–1336.

Pritchard, D. W. (1952). Salinity distribution and circulation in the Chesapeake Bay estuaries system. *Journal of Marine Research*, *11*, 106–123.

Rayson, M. D., Gross, E. S., Hetland, R. D., & Fringer, O. B. (2016). Time scales in Galveston Bay: An unsteady estuary. *Journal of Geophysical Research: Oceans*, *121*, 2268–2285. https://doi.org/10.1002/2015JC011181

Rosenberg, R. (1990). Negative oxygen trends in Swedish coastal bottom waters. *Marine Pollution Bulletin*, *21*(7), 335–339. https://doi.org/10.1016/0025-326X(90)90794-9

Ryan, H. F., Noble, M. A., Williams, E. A., & Gelfenbaum, G. (1997). Tidal current shear in a broad, shallow, river-dominated estuary. *Continental Shelf Research*, *17*(6), 665–688. https://doi.org/10.1016/S0278-4343(96)00053-2

Sanford, B. P., Boicourt, W. C., & Rives, S. R. (1992). Model for estimating tidal flushing of small embayments. *Journal of Waterway, Port, Coastal, and Ocean Engineering*, *118*(6), 635–654. https://doi.org/10.1061/(ASCE)0733-950X(1992)118:6(635)

Schroeder, W. W., Dinnel, S. P., & Wiseman, W. J. (1990). Salinity stratification in a river-dominated estuary. *Estuaries*, *13*(2), 145–154. https://doi.org/10.2307/1351583

Sheldon, J. E., & Alber, M. (2006). The calculation of estuarine turnover times using freshwater fraction and tidal prism models: A critical evaluation. *Estuaries and Coasts*, *29*(1), 133–146. https://doi.org/10.1007/BF02784705

Shen, J., & Haas, L. (2004). Calculating age and residence time in the tidal York River using three-dimensional model experiments. *Estuarine, Coastal and Shelf Science*, *61*(3), 449–461. https://doi.org/10.1016/j.ecss.2004.06.010

Shen, J., & Wang, H. V. (2007). Determining the age of water and long-term transport timescales of the Chesapeake Bay. *Estuarine, Coastal and Shelf Science*, *74*(4), 585–598. https://doi.org/10.1016/j.ecss.2007.05.017

Smith, R. (1977). Long-term dispersion of contaminants in small estuaries. *Journal of Fluid Mechanics*, *82*(1), 129–146. https://doi.org/10.1017/S0022112077000561

Stumpf, R. P., Gelfenbaum, G., & Pennock, J. R. (1993). Wind and tidal forcing of a buoyant plume, Mobile Bay, Alabama. *Continental Shelf Research*, *13*(11), 1281–1301. https://doi.org/10.1016/0278-4343(93)90053-Z

Takeoka, H. (1984). Fundamental concepts of exchange and transport time scales in a coastal sea. *Continental Shelf Research*, *3*(3), 311–326. https://doi.org/10.1016/0278-4343(84)90014-1

Turner, R. E., Schroeder, W. W., & Wiseman, W. M. Jr. (1987). The role of stratification in the deoxygenation of Mobile Bay and adjacent shelf bottom waters. *Estuaries*, *10*(1), 13–19. https://doi.org/10.2307/1352020

Valle-Levinson, A. (1995). Observations of barotropic and baroclinic exchanges in the lower Chesapeake Bay. *Continental Shelf Research*, *15*(13), 1631–1647. https://doi.org/10.1016/0278-4343(95)00011-O

Valle-Levinson, A. (2008). Density-driven exchange flow in terms of the Kelvin and Ekman numbers. *Journal of Geophysical Research*, *113*, C04001. https://doi.org/10.1029/2007JC004144

Viero, D. P., & Defina, A. (2016). Water age, exposure time, and local flushing time in semi-enclosed, tidal basins with negligible freshwater inflow. *Journal of Marine Systems*, *156*, 16–29. https://doi.org/10.1016/j.jmarsys.2015.11.006

Warner, J. C., Geyer, W. R., & Arango, H. G. (2010). Using a composite grid approach in a complex coastal domain to estimate estuarine residence time. *Computers & Geosciences*, *36*(7), 921–935. https://doi.org/10.1016/j.cageo.2009.11.008

Webb, B. M., & Marr, C. (2016). Spatial variability of hydrodynamic timescales in a broad and shallow estuary: Mobile Bay, Alabama. *Journal of Coastal Research*, *32*(6), 1374–1389.

Zhang, W. G., Wilkin, J. L., & Schofield, O. M. E. (2010). Simulation of water age and residence time in New York Bight. *Journal of Physical Oceanography*, *40*(5), 965–982. https://doi.org/10.1175/2009JPO4249.1

Zimmerman, J. T. F. (1976). Mixing and flushing of tidal embayments in the western Dutch Wadden Sea. Part I: Distribution of salinity and calculation of mixing time scales. *Netherlands Journal of Sea Research*, *10*(2), 149–191. https://doi.org/10.1016/0077-7579(76)90013-2

Zimmerman, J. T. F. (1988). Estuarine residence times. In B. Kierfve (Ed.), *Hydrodynamics of Estuaries*, *Estuarine Physics* (Vol. 1, pp. 75–84). Boca Raton, FL: CRC Press.